

**Dicke model with disordered spin-boson couplings**Pragna Das , Sebastian Wüster , and Auditya Sharma *Indian Institute of Science Education and Research, Bhopal 462066, India* (Received 24 August 2023; revised 10 November 2023; accepted 21 December 2023; published 18 January 2024)

We introduce and study the disordered Dicke model in which the spin-boson couplings are drawn from a random distribution with some finite width. Regarding the quantum phase transition, we show that, when the standard deviation  $\sigma$  of the coupling strength gradually increases, the critical value of the mean coupling strength  $\mu$  gradually decreases, and after a certain  $\sigma$  there is no quantum phase transition at all; the system always lies in the superradiant phase. We derive an approximate expression for the quantum phase transition in the presence of disorder in terms of  $\mu$  and  $\sigma$ , which we numerically verify. Studying the thermal phase transition in the disordered Dicke model, we obtain an analytical expression for the critical temperature in terms of the mean and standard deviation of the coupling strength. We observe that, even when the mean of the coupling strength is zero, there is a finite temperature transition if the standard deviation of the coupling is sufficiently high. Disordered couplings in the Dicke model will exist in quantum dot superlattices, and we also sketch how they can be engineered and controlled with ultracold atoms or molecules in a cavity.

DOI: [10.1103/PhysRevA.109.013715](https://doi.org/10.1103/PhysRevA.109.013715)**I. INTRODUCTION**

The Dicke model [1], which describes the interaction between light and matter, is of fundamental importance within the field of quantum optics. It exhibits a variety of interesting phase transitions covering quantum phase transitions [2–6] (QPT), excited-state quantum phase transitions [7,8] (ES-QPT), and thermal phase transitions [7–11] (TPT). The QPT takes place in the thermodynamic limit of infinite atom number  $N \rightarrow \infty$ , where the system goes from the normal phase (NP) to the superradiant phase (SP) [12] at some critical coupling strength  $g_c$  [3] between spins and bosons. If temperature is introduced to the system, for  $g > g_c$ , there is a critical temperature  $T_c$ , above which the system returns to the NP from the SP, whereas for  $g < g_c$  the system lies in the NP for all temperatures [7–9,13–16].

Here, we generalize the standard Dicke model towards disorder in the coupling strength  $g$  for which we propose several practical realizations. While the role of disorder in the more general spin-boson model has been considered both in theoretical [17–24] and experimental [25–27] studies, the exploration of disorder-induced phenomena within this context is still at a nascent stage. The earlier work mainly focused on the study of polariton physics whereas we show that, if we introduce disorder with a sufficiently broad distribution into the coupling strength between spins and bosons, there exists a QPT (or at least a cross over) as well as a TPT even for vanishing mean coupling. We study mutual information [28–30] between two spins as a function of temperature whose usefulness was demonstrated for clean Dicke models previously [8,31]. We investigate our system both analytically and numerically, with results in agreement. Additionally, we propose experimental platforms with ultracold atoms or molecules in a cavity, which can confirm our results.

In the usual clean Dicke model, it is well known that the QPT [2–6] occurs at some critical light matter coupling strength. We find that, for the disordered Dicke model, both

the mean and the standard deviation of the random coupling distribution play a crucial role in the QPT. If either one of them or both are high, then the ground state exhibits superradiant behavior. To show this, we numerically calculate the ground-state energy and average boson number as a function of the coupling distribution for the disordered Dicke model. We show how a symmetry of the Hamiltonian can be exploited along with a heuristic argument to obtain the line of quantum criticality in an accurate manner.

To understand the thermal phase transition, we follow methods for which the basis was laid in Refs. [9,32], and calculate the partition function of the disordered Dicke model to obtain the critical temperature in terms of the disorder coupling strength. Numerically we calculate the mutual information between two spins for the disordered Dicke model by a method similar to our earlier work [8] for the usual Dicke model. When the width of the disorder is sufficiently high, there is a finite temperature transition from the SP to the NP even if the mean of the coupling strength is zero. We can predict the critical temperature of this transition analytically, signatures for which are also seen in the mutual information found numerically.

Earlier studies of disorder in the Dicke model considered the multimode case [33]. In contrast, we sketch several possible realizations of disorder in the *single-mode* Dicke model. It can naturally arise in semiconductor quantum dot lattices (see for, e.g., Ref. [34]), where each quantum dot can have a varied orientation relative to propagating electric fields, yet due to the small structure all dots effectively radiate into a single mode, causing superradiance. One can also engineer controlled realizations by transforming a random spatial distribution of atoms within an optical cavity [35] relative to a varying electric field amplitude into a distribution of couplings. Other possibilities include ultracold molecules whose fixed transition dipoles are randomly oriented with respect to the cavity field direction.

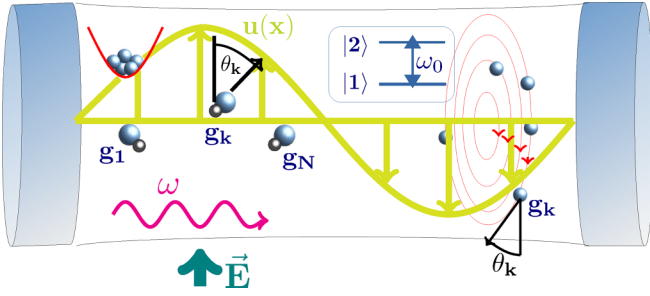


FIG. 1. Schematic of the disordered Dicke model where  $N$  two-level atoms are coupled to a single-mode bosonic field with different spin-boson coupling strengths  $g_k$  and two possible realizations. The frequency of the bosonic mode is  $\omega$  and the gap between two levels  $|1\rangle$  and  $|2\rangle$  of each atom is  $\omega_0$ . (left) These could be ultracold molecules whose fixed transition dipoles are randomly oriented with regard to (wrt) the cavity field direction (green) or (right) atoms under the influence of an additional external field that breaks their symmetry, such as the magnetic field around a wire (red).

The organization of the article is as follows. In the next section we will discuss the system Hamiltonian for the disordered Dicke model. In Secs. III and IV we present our results regarding the two types of phase transitions: QPT and TPT. In Sec. V we outline several possible experimental realisations. Finally in Sec. VI we provide a summary of our work.

## II. MODEL HAMILTONIAN AND QUANTIFIERS

In Fig. 1 we show a schematic of the disordered Dicke model. The Hamiltonian consists of a single-mode bosonic field coupled to  $N$  atoms with a coupling strength that is modeled as a random variable. The Hamiltonian can be written as

$$H = \omega a^\dagger a + \frac{\omega_0}{2} \sum_{i=1}^N \sigma_z^{(i)} + \frac{1}{\sqrt{N}} (a^\dagger + a) \sum_{i=1}^N g_i \sigma_x^{(i)}, \quad (1)$$

where the operators  $a$  and  $a^\dagger$  are the bosonic annihilation and creation operators, respectively, following the commutation relation  $[a, a^\dagger] = 1$ , and the  $N$  spin-1/2 atoms are described by Pauli matrices  $\sigma_{x,z}^{(i)}$  acting on site  $i$ . Here, the  $g_i$ 's are random numbers drawn from two types of distributions. In the first distribution, the  $g_i$ 's are drawn from a uniform unit box distribution with finite width ( $2\epsilon$ ) and height  $A$  such that  $2\epsilon A = 1$ . The parameters  $\epsilon$  and  $A$  are chosen so that  $2\epsilon = (\mu + \epsilon) - (\mu - \epsilon)$ ,  $\epsilon = \sqrt{3}\sigma$ , and hence  $A = \frac{1}{2\sqrt{3}\sigma}$  where  $\mu$  and  $\sigma$  are the mean and the standard deviation. In the second distribution, we consider  $g_i \propto \cos \theta_i$ , where  $\theta_i$  are angles randomly drawn from a Gaussian distribution  $p(\theta) \sim \exp[-(\theta - \theta_0)^2 / \sigma_\theta^2]$ . Both can be engineered, e.g., in optical cavities as sketched in Fig. 1 and discussed in Sec. V. Due to the disorder in the coupling strengths, the total angular momentum is not a conserved quantity of the Hamiltonian 1 and hence we have to consider all possible spin configurations. For  $N$  spins, the corresponding dimension of the spin subspace is  $2^N$  and the bosonic subspace dimension is  $n_{\max} + 1$ , where  $n_{\max}$  is the maximal occupation we allow for the bosonic field. Hence the total Hilbert space dimension for our numerical calculations is  $N_D = 2^N (n_{\max} + 1)$ .

In the next sections we explore the QPT and TPT separately, based on the properties of eigenvalues and eigenstates of Eq. (1). We study useful quantifiers such as ground-state energy, average boson number, and mutual information between two spins. For a mixed state (like a temperature equilibrated state), the mutual information has been shown [8] to be an appropriate quantity, although it contains both quantum and classical correlations. We shall study the mutual information [8,28–30,36] between two spins which are in a mixed density matrix that is determined from the state of the overall system. Defining the reduced density matrices of any two selected spins to be  $\rho_1$  and  $\rho_2$  and the reduced density matrix corresponding to the two-spin state to be  $\rho_{12}$ , the mutual information between the two spins can be computed using the relation

$$I_{12} = S_1 + S_2 - S_{12}, \quad (2)$$

where  $S_{1,2} = -\text{Tr}[\rho_{1,2} \ln(\rho_{1,2})]$ ,  $S_{12} = -\text{Tr}[\rho_{12} \ln(\rho_{12})]$  are the corresponding von Neumann entropies. Since we will be interested in  $I_{12}$  at finite temperature, we will first construct the total thermal density matrix  $\rho_{\text{Th}} = e^{-\frac{H}{k_B T}}$ , and then trace over the bosonic subspace and the remaining  $(N - 2)$  or  $(N - 1)$  spins. Since we will average over the disorder, it does not matter which two spins are considered for the purpose of computing mutual information. Another useful observable that we employ to study the QPT is the average boson number  $\langle a^\dagger a \rangle$  evaluated in the interacting ground state.

## III. QUANTUM PHASE TRANSITION

It is well known that in the thermodynamic limit (when the atom number  $N \rightarrow \infty$ ), the usual Dicke model exhibits a quantum phase transition [4] from the normal phase to the superradiant phase at some critical coupling strength  $g_c$ . In the disordered Dicke model, if we fix the mean of the coupling strength at a sufficiently low value and vary the standard deviation ( $\sigma$ ) we see a similar QPT. The QPT here is studied with the aid of the disorder-averaged energy and average boson number in the ground state. In Figs. 2 and 3 we show these properties in the ground state of the disordered Dicke model, considering two types of distributions as discussed in the previous section.

What we will empirically show now is that much of the behavior of the disordered Dicke model can be understood by averaging the known results for the disorder-free (clean) model. This is not clear *a priori* since all the two-level systems in the disordered model couple to the same bosonic mode and thus get coupled. For the clean Dicke model, Emary *et al.* [2] derived analytical results for the ground-state energy

$$E_G = \begin{cases} -\frac{N\omega_0}{2}, & g < g_c, \\ -\frac{N\omega_0}{4} \left[ \frac{g^2}{g_c^2} + \frac{g_c^2}{g^2} \right], & g > g_c, \end{cases} \quad (3)$$

and the average boson number in the cavity

$$\langle a^\dagger a \rangle = \begin{cases} 0, & g < g_c, \\ \frac{N}{\omega^2} \left[ g^2 - \frac{g_c^4}{g^2} \right], & g > g_c, \end{cases} \quad (4)$$

where  $g_c$  is the critical value of the coupling in the absence of disorder. We will make use of the above results and integrate

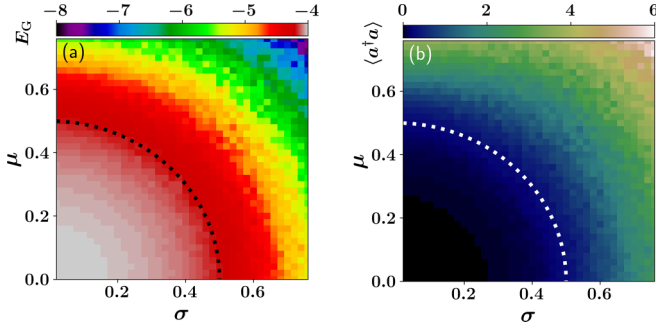


FIG. 2. Phase diagram of the disordered Dicke model with uniform coupling distribution [Eq. (8)]. To map it out, we show (a) the ground-state energy  $E_G$  and (b) the average boson number,  $\langle a^\dagger a \rangle$  wrt the ground state, as a function of the standard deviation  $\sigma$  and the mean  $\mu$  of the coupling parameters  $g_i$ . We consider the resonant case  $\omega = \omega_0 = 1$ , take the average over 120 realizations, fix the atom number to be  $N = 8$ , and the bosonic cutoff to be  $n_{\max} = 40$ . Here the dotted line is the critical line for the QPT:  $\sqrt{\mu^2 + \sigma^2} = g_c$  [see Eq. (7)].

over the coupling strength distribution to obtain approximate analytical results for the disordered Dicke model. We denote the disorder-averaged value of an observable  $O$  as  $\bar{O}$ :

$$\bar{O} = \int_{x_1}^{x_2} P(g)O(g)dg, \quad (5)$$

where  $P(g)$  is the distribution of the disorder and the limits of integration  $x_1$  and  $x_2$  have to be chosen appropriately according to the observable and the distribution being considered.

For the disorder-free Dicke model, the transition from the NP to the SP happens at the critical coupling strength  $g_c$ . Since the disordered Dicke model is described by two parameters  $\mu$  and  $\sigma$ , we would expect a line that would separate the NP and the SP in the  $\mu$ - $\sigma$  plane. A crude guess to obtain this line would be to look for points where the average coupling

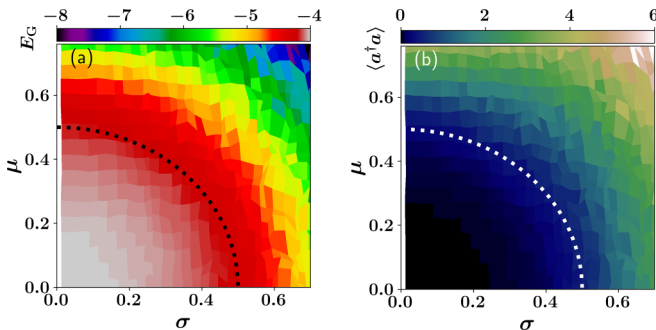


FIG. 3. Phase diagram of the disordered Dicke model where  $g_i = 2 \cos \theta_i$ ,  $\theta_i$  are angles randomly drawn from a Gaussian distribution with mean  $\theta_0$  and standard deviation  $\sigma_\theta$ . To map it out, we show (a) the ground-state energy  $E_G$  and (b) the average boson number,  $\langle a^\dagger a \rangle$  wrt the ground state as a function of the standard deviation  $\sigma$  and the mean  $\mu$  of the coupling parameters  $g_i$ . We consider the resonant case  $\omega = \omega_0 = 1$  and take the average over 200 realizations, fix the atom number to be  $N = 8$ , and the bosonic cutoff to be  $n_{\max} = 40$ . Here the dotted line is the critical line for the QPT:  $\sqrt{\mu^2 + \sigma^2} = g_c$  [see Eq. (7)].

$\langle g \rangle$  equals  $g_c$ . A refined argument, incorporating a symmetry of the Hamiltonian, yields an excellent approximation for the critical line. We observe that the Hamiltonian in Eq. (1) has the same eigenvalues as one in which any one of the couplings  $g_i$  is changed to  $-g_i$ . In other words, the eigenvalues of  $H(\{g_j, j \neq i\}, g_i)$  and  $H(\{g_j, j \neq i\}, -g_i)$  are the same. This is a direct consequence of the fact that

$$H(\{g_j, j \neq i\}, -g_i) = \sigma_i^z H(\{g_j, j \neq i\}, g_i) \sigma_i^z. \quad (6)$$

Thus when the transformation  $T = \sigma_i^z$  is applied on any eigenstate of the Hamiltonian  $H(\{g_j, j \neq i\}, g_i)$ , we would get an eigenstate of the Hamiltonian  $H(\{g_j, j \neq i\}, -g_i)$  with the same eigenvalue. This argument naturally extends to the case when multiple  $g_i$ 's undergo a sign change. Hence we can consider a scenario where all the coupling strengths are made positive, i.e., if there are any negative coupling strengths we may simply take their absolute values. Thus the root-mean-squared value of the coupling is really the typical coupling of this system. Hence the critical line can be written as  $\sqrt{\langle g^2 \rangle} = g_c$ , i.e.,

$$\sqrt{\mu^2 + \sigma^2} = g_c. \quad (7)$$

We show below that this result agrees very closely with the exact numerical results for two different distributions. Moreover, we will show in the next section that the above approximate result can be recovered with the aid of a suitable limiting procedure from our result for the thermal phase transition temperature.

### A. Uniform distribution

In the first scenario the coupling  $g$  is drawn from a uniform distribution

$$P_u(g) = \begin{cases} \frac{1}{2\sqrt{3}\sigma} & \text{if } \mu - \sqrt{3}\sigma < g < \mu + \sqrt{3}\sigma, \\ 0 & \text{otherwise,} \end{cases} \quad (8)$$

with mean  $\mu$  and standard deviation  $\sigma$ .

The disorder-averaged ground-state energy and average boson number are found from the integrals

$$\bar{E}_G = \int_{x_1}^{x_2} P_u(g) E_G dg, \quad (9)$$

$$\overline{\langle a^\dagger a \rangle} = \int_{x_1}^{x_2} P_u(g) \langle a^\dagger a \rangle dg, \quad (10)$$

where  $E_G$  is given in Eq. (3),  $\langle a^\dagger a \rangle$  is given in Eq. (4), and we use the overline to denote the disorder average. The lower and upper limits of the box distribution are  $x_1 = \mu - \sqrt{3}\sigma$  and  $x_2 = \mu + \sqrt{3}\sigma$ , respectively, and we consider  $\mu$  and  $\sigma$  to be in the range  $[0,1]$ . Figure 2(a) shows the numerical value of the ground-state energy  $E_G$  of the system as a function of the standard deviation ( $\sigma$ ) and mean ( $\mu$ ) of the coupling parameter. In this figure the white or pink color indicates the normal phase where the ground-state energy is large and constant  $E_G = -\frac{N\omega_0}{2}$  and the other colors represent the superradiant phase where  $E_G$  is decreasing. Similarly, Fig. 2(b) shows the average boson number in the ground state of the disordered Dicke model. In the normal phase  $\overline{\langle a^\dagger a \rangle} \approx 0$  (black color), i.e., there are no excitations in the bosonic mode whereas in the

superradiant phase  $\overline{\langle a^\dagger a \rangle}$  is finite (other colors), which indicates a macroscopic excitation of the bosonic mode. The dotted line in Fig. 2 which separates the NP and SP for the QPT is obtained using Eq. (7). We note that our numerical data obtained for a system with a small  $N$  agree with this critical line quite well. It is clear that for  $\mu = 0$ , the standard deviation of the disordered Dicke model plays the same role as the coupling parameter  $g$  in the usual Dicke model and the critical point is Eq. (7).

While the critical line is well described by Eq. (7) when the number of atoms is small, corrections would be expected as  $N$  is made large (thermodynamic limit). In Appendix A with the aid of analytical expressions obtained by disorder-averaging the clean Dicke model results, we generate data for intensive quantities (energy per atom), so the dependence on  $N$  is removed. We also discuss how to obtain improved estimates for the critical line that separates the NP and SP. The robustness of our numerical results as the bosonic cutoff  $n_{\max}$  is increased is shown in Appendix B. Thus, while a directly numerical demonstration of nonanalytic behavior for the disordered Dicke model is intractable, we offer plausible numerical evidence to show that the behavior of the disordered Dicke model across the phase boundaries is quite similar to that of the usual Dicke model, where the criticality has been established.

### B. Gaussian distribution

To demonstrate the robustness of our results to variations of the detailed shape of the probability distribution for the coupling, we now consider a second case. The angle  $\theta$  is drawn from the Gaussian distribution

$$P(\theta) \propto e^{-(\theta - \theta_0)^2 / \sigma_\theta^2}, \quad (11)$$

where  $\theta_0 \in [0, \pi]$  is the mean and  $\sigma_\theta \in [0, \frac{\pi}{4}]$  is the standard deviation of  $\theta$  and the disordered coupling strength for the  $i$ th spin is then taken as

$$g_i = 2 \cos \theta_i. \quad (12)$$

Here, we numerically calculate the mean and the standard deviation of  $g$ :  $\mu = \langle g \rangle = \frac{1}{N} \sum_{i=1}^N g_i$  and  $\sigma = \sqrt{\langle g^2 \rangle - \langle g \rangle^2}$  to obtain characteristics of the distribution that are easily comparable with the previous section. The ground-state energy  $E_G$  and the average boson number for this distribution are shown in Fig. 3 and we see a behavior similar to the uniform distribution used in Fig. 2. The dotted line sketched using Eq. (7) is seen to be an excellent representation of the line that separates the NP from the SP.

### IV. THERMAL PHASE TRANSITION

Moving from the quantum to the thermal phase transition, in this section we derive an analytical expression for the critical temperature for the disordered Dicke model building on previous results [9,32] for the clean Dicke model. We start by rewriting the system Hamiltonian for the disordered Dicke

model as

$$\begin{aligned} \tilde{\mathcal{H}} &= \frac{\mathcal{H}}{\omega} \\ &= a^\dagger a + \sum_{j=1}^N \frac{\epsilon}{2} \sigma_j^z + \frac{1}{\sqrt{N}} (a + a^\dagger) \sum_{j=1}^N \lambda_j \sigma_j^x \\ &= a^\dagger a + \sum_{j=1}^N h_j, \end{aligned} \quad (13)$$

where  $\epsilon = \frac{\omega_0}{\omega}$ ,  $\lambda_j = \frac{g_j}{\omega}$ , and

$$h_j = \frac{\epsilon}{2} \sigma_j^z + \frac{1}{\sqrt{N}} (a + a^\dagger) \lambda_j \sigma_j^x. \quad (14)$$

Following Wang and Hieo [9] who studied the Dicke model within the rotating wave approximation, the partition function can be computed as

$$\begin{aligned} Z(N, T) &= \sum_{s_1, \dots, s_N = \pm 1} \int \frac{d^2 \alpha}{\pi} \langle s_1 \dots s_N | \langle \alpha | e^{-\beta \tilde{\mathcal{H}}} | \alpha \rangle | s_1 \dots s_N \rangle \\ &= \int \frac{d^2 \alpha}{\pi} e^{-\beta |\alpha|^2} \prod_{j=1, 2, \dots, N} \langle s_j | e^{-\beta h_j} | s_j \rangle \\ &= \int \frac{d^2 \alpha}{\pi} e^{-\beta |\alpha|^2} \prod_{j=1, 2, \dots, N} \\ &\quad \times \left( 2 \cosh \left[ \frac{\beta \epsilon}{2} \left[ 1 + \frac{16 \lambda_j^2 \alpha^2}{\epsilon^2 N} \right]^{1/2} \right] \right). \end{aligned} \quad (15)$$

Here  $|\alpha\rangle$  is a coherent state which satisfies the relation  $a|\alpha\rangle = \alpha|\alpha\rangle$  and  $|s_1 \dots s_N\rangle$  is the product basis for the spin subspace. In polar coordinates the partition function becomes

$$\begin{aligned} Z(N, T) &= \int_0^\infty r dr e^{-\beta r^2} \prod_{j=1, 2, \dots, N} \\ &\quad \times \left( 2 \cosh \left[ \frac{\beta \epsilon}{2} \left[ 1 + \frac{16 \lambda_j^2 r^2}{\epsilon^2 N} \right]^{1/2} \right] \right). \end{aligned} \quad (16)$$

Defining the variable  $y = \frac{r^2}{N}$  allows us to rewrite the above integral as

$$\begin{aligned} Z(N, T) &= N \int_0^\infty dy e^{-\beta N y} \prod_{j=1, 2, \dots, N} \\ &\quad \times \left( 2 \cosh \left[ \frac{\beta \epsilon}{2} \left[ 1 + \frac{16 \lambda_j^2 y}{\epsilon^2} \right]^{1/2} \right] \right) \\ &= N \int_0^\infty dy \exp \left( -\beta N y + \sum_{j=1}^N \ln \right. \\ &\quad \left. \times \left[ \left( 2 \cosh \left[ \frac{\beta \epsilon}{2} \left[ 1 + \frac{16 \lambda_j^2 y}{\epsilon^2} \right]^{1/2} \right] \right) \right] \right). \end{aligned} \quad (17)$$

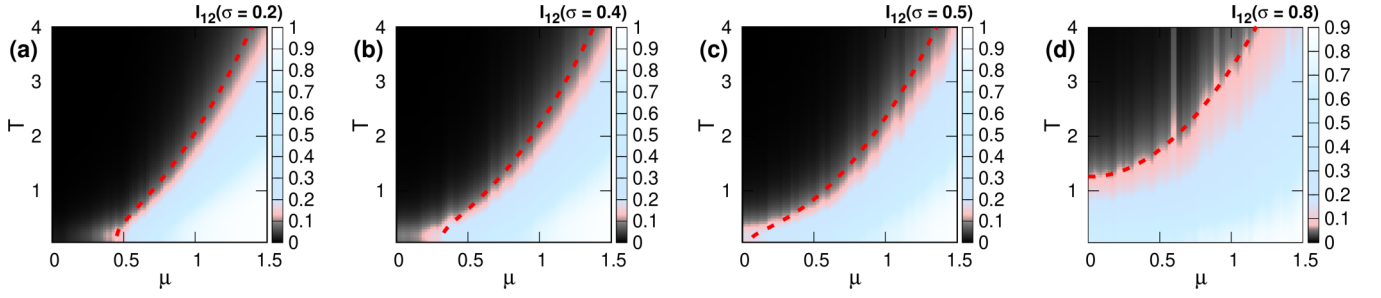


FIG. 4. Thermal phase diagrams of the disordered Dicke model, based on the mutual information between two spins. Axes are the temperature  $T$  and mean coupling strength  $\mu = \langle g \rangle$ , for (a)  $\sigma = 0.2$ , (b)  $\sigma = 0.4$ , (c)  $\sigma = 0.5$ , and (d)  $\sigma = 0.8$ . The couplings  $g$  are drawn from a random uniform distribution with finite mean  $\mu$  and standard deviation  $\sigma$  [see Eq. (8)]. The number of atoms is  $N = 6$  and we choose the bosonic cutoff as  $n_{\max} = 40$ . We take the average over 150 realizations of  $g$  for each  $\sigma$ .

We can write this more compactly as

$$Z(N, T) = N \int_0^\infty dy \exp(\phi_N(y)) \quad (18)$$

using a shorthand

$$\begin{aligned} \phi_N(y) = & -\beta N y \\ & + \sum_{j=1}^N \ln \left[ \left( 2 \cosh \left[ \frac{\beta \epsilon}{2} \left[ 1 + \frac{16 \lambda_j^2 y}{\epsilon^2} \right]^{1/2} \right] \right) \right] \end{aligned}$$

for the exponent. We would like to evaluate the above integral using the method of steepest descent for which we would like to extract the point at which  $\phi_N(y)$  is a maximum. To find this, we compute the derivative

$$\frac{d\phi_N(y)}{dy} = -\beta N + \frac{4\beta}{\epsilon} \sum_j \frac{\lambda_j^2}{\eta_j} \tanh\left(\frac{\beta \epsilon \eta_j}{2}\right), \quad (19)$$

where we use the shorthand notation

$$\eta_j = \left[ 1 + \frac{16 \lambda_j^2 y^2}{\epsilon} \right]^{1/2}. \quad (20)$$

A vanishing derivative  $\frac{d\phi_N(y)}{dy} = 0$  implies

$$0 = -\beta N + \frac{4\beta}{\epsilon} \sum_j \frac{\lambda_j^2}{\eta_j} \tanh\left(\frac{\beta \epsilon \eta_j}{2}\right). \quad (21)$$

Following the intuition from the corresponding calculation for the clean Dicke model, we argue that the critical value of the inverse temperature must correspond to the case when all the  $\eta_j$  take their minimum possible value, namely, unity. Inserting  $\eta_j = 1$ , we have

$$0 = -\beta_c N + \frac{4\beta_c}{\epsilon} \sum_j \lambda_j^2 \tanh\left(\frac{\beta_c \epsilon}{2}\right), \quad (22)$$

which can be reshaped into

$$\sum_j \lambda_j^2 \tanh\left(\frac{\beta_c \epsilon}{2}\right) = \frac{N \epsilon}{4}. \quad (23)$$

This gives us

$$\tanh\left(\frac{\beta_c \epsilon}{2}\right) = \frac{\epsilon}{4 \frac{\sum \lambda_j^2}{N}} = \frac{\epsilon}{4 \langle \lambda^2 \rangle}. \quad (24)$$

Substituting for the expressions for  $\epsilon$  and  $\lambda$ , we obtain an expression for the transition temperature

$$T_c = \frac{\omega_0}{2\omega} \frac{1}{\tanh^{-1}\left(\frac{\omega_0 \omega}{4 \langle g^2 \rangle}\right)}. \quad (25)$$

To verify this expression for the critical temperature, we numerically study the mutual information between two spins, which has been shown to be a useful marker for the thermal phase transition in the Dicke model [8,31]. In Fig. 4, we show the mutual information between two spins as a function of the mean coupling strength  $\mu$  and the temperature  $T$  for different standard deviations  $\sigma = 0.2, 0.4, 0.5, 0.8$ . For  $\sigma = 0.2$  the phase diagram is almost identical to the one for the usual Dicke model (see Fig. 4(c) of our earlier work [8]). For  $\mu < \frac{1}{2}$  the system lies in the normal phase, which gives rise here to the black color; for  $\mu > \frac{1}{2}$ , there is a thermal phase transition from the superradiant phase (light color) to the normal phase around some critical temperature. In this figure the red dashed line denotes the analytical critical temperature of Eq. (25). We can see that it describes the numerical results well. If the standard deviation is increased, it is clear from Figs. 4(b) ( $\sigma = 0.4$ ) and 4(c) ( $\sigma = 0.5$ ) that the thermal phase transition starts at lower mean values  $\mu$  than  $\mu = g_c$ . Finally, for sufficiently wide coupling distributions, with, e.g.,  $\sigma = 0.8$ , there is a clear TPT from the SP to the NP even for vanishing mean coupling strength  $\mu = \langle g \rangle = 0$ . Hence, we can conclude from Fig. 4 that if we introduce disorder with a sufficiently broad distribution into the coupling strength between spins and bosons, there exists a TPT even for vanishing mean coupling  $\mu = \langle g \rangle = 0$ .

In Fig. 5, we show similar data, but using the distribution based on angles, Eq. (11) and Eq. (12). We again show the mutual information between two spins as a function of the mean and the standard deviation of the spin-boson coupling strength for fixed temperatures. Here  $\theta$  is a random number, drawn from a Gaussian distribution and  $g = 2 \cos \theta$  which we describe in the Sec. III B. In the normal phase the mutual information is small, shown by the black color. However, in the superradiant phase  $I_{12}$  is relatively high, which is rep-

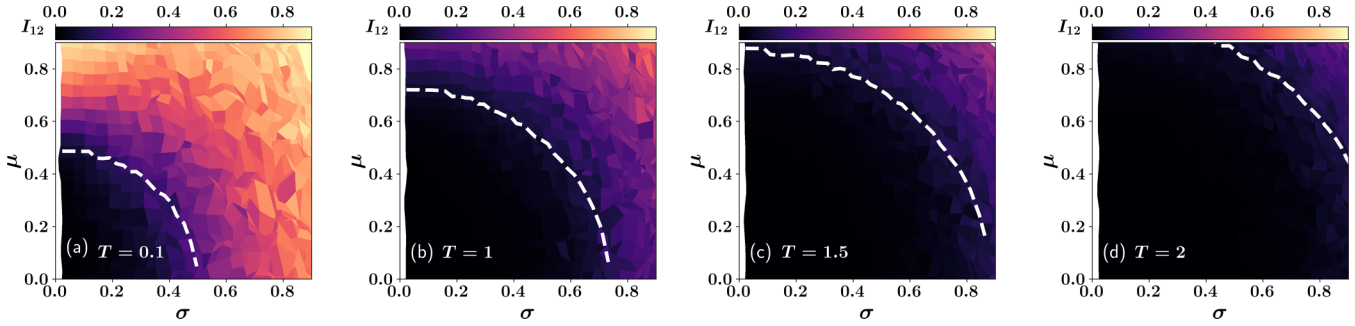


FIG. 5. Thermal phase diagrams of the disordered Dicke model, based on the mutual information between two spins. Axes are the standard deviation  $\sigma$  and mean coupling strength  $\mu = \langle g \rangle$  for (a)  $T = 0.1$ , (b)  $T = 1$ , (c)  $T = 1.5$ , and (d)  $T = 2$ . The couplings  $g_i = 2 \cos \theta_i$ , where  $\theta_i$  are angles randomly drawn from a Gaussian distribution with mean  $\theta_0$  and standard deviation  $\sigma_\theta$ . The number of atoms is  $N = 6$  and we choose the bosonic cutoff as  $n_{\max} = 40$ . We take the average over 96 realizations of  $g$  for each temperature.

represented by the other colors. One can notice that, when we gradually increase the temperature, the normal phase is also expanding in parameter space. In this figure the white dashed curves represent the critical values of  $\sigma$  and  $\mu$  for TPT that we derived analytically in Eq. (25), which separate the normal and superradiant phases quite well.

We now show how to recover Eq. (7) from Eq. (25). Inserting  $T_c = 0$ , we have

$$\frac{\omega_0 \omega}{4 \langle g^2 \rangle} = \tanh(\infty) = 1. \quad (26)$$

Thus the critical line for the QPT is given by

$$\sqrt{\langle g^2 \rangle} = g_c = \frac{\sqrt{\omega \omega_0}}{2}, \quad (27)$$

which is the same as Eq. (7).

## V. REALIZING DISORDERED COUPLINGS IN DICKE MODEL WITH COLD ATOM OR ULTRACOLD MOLECULES IN A CAVITY

While we intentionally study the abstract model (1) such that it can apply to a variety of systems, we provide in this section some examples for practical realisations. When considering the origin of the Hamiltonian (1) through light matter coupling for two-level systems in a single-mode optical cavity, one has, in the dipole approximation [37]

$$g_i = \sqrt{\frac{1}{2\hbar\epsilon_0\omega}} \omega_0 u(\mathbf{x}_i) d_{21} \cos \theta_i, \quad (28)$$

where  $\epsilon_0$  is the vacuum permeability,  $u(\mathbf{x}_i)$  the cavity mode amplitude at the location  $\mathbf{x}_i$  of the  $i$ th two level system, and  $d_{21} \cos \theta_i$  the transition dipole matrix element between  $|2\rangle$  and  $|1\rangle$  projected onto the local cavity field axis, where we made the dependence on the angle  $\theta_i$  between cavity field at  $\mathbf{x}_i$  and transition dipole axis explicit.

Even for identical atoms or molecules, treated as an approximate two-level system (TLS), a random position distribution  $\mathbf{x}_i$  can now translate into disordered coupling strengths through the position of the TLS relative to the cavity field structure in  $u(\mathbf{x}_i)$  that may contain standing waves, which will cause disorder in the field strength. While this can easily be avoided by trapping all atoms on spatial

scales small compared to the cavity wavelength [38], one can just as well generate a range of coupling distributions by weakly trapping the atoms on the flanks of a standing wave [39]. For atomic TLSs without any external fields other than the cavity field, there would be no additional contribution from the transition dipole orientation since we can always choose the quantization axis along the local cavity-mode electric field direction, such that  $\cos \theta_i \rightarrow 1$ . This is no longer true once an additional external field perturbs the symmetry, or the particle is asymmetric, such as most molecules are.

A symmetry-breaking field  $\mathbf{B}$  could be magnetic, strong enough to Zeeman-shift undesired magnetic sublevels of the excited state out of cavity resonance and locally defining the quantisation axis. If the cavity is penetrated, for example, by the circular magnetic field around a current carrying wire, a random three-dimensional (3D) distribution of atomic positions will translate into a random distribution of angles between quantisation axis and cavity mode electric field, and hence affect couplings, as sketched in Fig. 1.

Another approach to break the symmetry of the two-level system would be considering ultracold molecules [40,41] in the optical cavity [42]. Typical heteronuclear molecules possess transition dipole moments with a fixed orientation relative to the molecular axis [43]. Molecules oriented randomly in three dimensions, such as in the ground state with angular momentum  $J = 0$  of the quantum mechanical rotor, will thus exhibit a distribution of couplings. The disadvantages of molecules are their vibrational and rotational degrees of freedom, which are undesired here. However eliminating or minimizing the impact of these is also required for quantum information and quantum simulation applications of ultracold molecules and aids cooling them and is thus being actively pursued. Coupling to both degrees of freedom can be strongly suppressed, by choosing a molecule with a nearly diagonal Franck-Condon factor [44] between the ground and excited states, and a larger angular momentum in the ground state than the excited state [45,46].

Randomly oriented molecules neatly realize the uniform coupling distribution that we focused on since the probability of a given polar angle  $\theta$  is  $P(\theta) = \frac{\sin \theta}{2}$  and hence  $P(\cos \theta)$  will be uniform. Refined distributions can then be tailored by partially orienting molecules along the cavity field axis,

e.g.,  $P(\theta) = \mathcal{N}e^{-(\theta-\theta_0)^2/\sigma_\theta^2}$ , with  $\theta_0$  enforced by an additional external bias field  $\mathbf{E}$  (see Fig. 1).

The implementations of the disordered Dicke model with cold atoms and molecules in cavities that we discussed above can then provide controlled insight, which can be leveraged for understanding the underlying Hamiltonian in more complex and less controlled cases, such as when studying superradiance effects in semiconductor quantum dot lattices [34]. In this case of transition dipoles of carriers in quantum dots are also likely disordered by additional fields and quantum dot geometries, however, a clear distinction of such effects from other disorder and decoherence sources will be much more difficult.

## VI. SUMMARY AND CONCLUSION

In this work, we propose and investigate a disordered single-mode Dicke model. We specifically focus on two concrete random distributions of the spin-boson coupling parameters  $g_i$ : (i) a uniform distribution and (ii)  $g_i \propto \cos \theta_i$ , where  $\theta_i$  are Gaussian random variables and study the resulting quantum and thermal phase transitions in the disordered Dicke model. In both cases we see similar results and hence demonstrate that our results are robust to changes in the detailed shape of the distribution.

We find that the phase transitions depend on both the mean and the standard deviation of the random coupling strengths. For the QPT, we find that, for mean coupling strengths significantly smaller than their standard deviation  $\sigma$ , the standard deviation plays a role similar to the coupling  $g$  in the clean Dicke model. Even for vanishing mean coupling  $\mu = 0$ , the system thus shows a QPT around  $\sigma = g_c$  for uniformly distributed couplings. When  $\mu$  is systematically increased, the critical value of  $\sigma$  decreases, and after a certain mean coupling ( $= g_c$ ) the QPT disappears. We show that the critical line is well described by  $\sqrt{\mu^2 + \sigma^2} = g_c$  when the number of atoms is small. This corresponds to simply equating the root mean squared (rms) coupling to the critical value of the

undisordered model, and is able to delineate the boundary between the phases quite well. Moreover, we are able to recover this result by taking the zero transition temperature limit of the expression for the thermal phase transition. In the Appendix, with the aid of analytical expressions obtained by disorder-averaging the clean Dicke model results, we also discuss how to obtain improved estimates for the critical line that separates the NP and SP.

We also derive an analytical expression for the critical temperature and numerically verify it with the aid of mutual information between two spins. It shows that, for wide distributions, such that  $\sigma$  is large, there is a phase transition from SP to NP at  $\sigma \approx 0.8$  even for vanishing mean coupling strength  $\mu = 0$ .

The disordered Dicke model should describe quantum dot superlattices in semiconductor quantum optics (see, e.g., Ref. [34]). Additionally, we list several methods by which the disordered Dicke model can be realized in experiments with ultracold atoms or molecules in a cavity.

## ACKNOWLEDGMENTS

We are grateful to the High Performance Computing (HPC) facility at IISER Bhopal, where large-scale calculations in this project were run. P.D. is grateful to IISERB for the Ph.D. fellowship. A.S. acknowledges financial support from SERB via the Grant No. CRG/2019/003447, and from DST via the DST-INSPIRE Faculty Award No. DST/INSPIRE/04/2014/002461.

## APPENDIX A: UNIFORM DISTRIBUTION

Consider the scenario where the coupling  $g$  is drawn from a uniform distribution which is given in Eq. (8) in the main text. Carrying out the integration in Eq. (10) we have the disorder-averaged value of the energy and average boson number of the ground state. Depending on the relation between  $x_1$ ,  $x_2$ , and  $g_c$ , there are five cases to be considered. After performing the integration outlined above, we obtain an expression for the disorder-averaged ground-state energy

$$\frac{\overline{E_G}}{N} = \begin{cases} D_1 \left[ \frac{2g_c}{3} - \frac{x_1^3}{3} + \frac{g_c^4}{x_1} \right] - \frac{\omega_0}{2} \left( \frac{x_2 + g_c}{2\sqrt{3}\sigma} \right), & x_1 < -g_c \text{ and } 0 < x_2 \leq g_c, \\ D_1 \left[ \frac{4g_c^3}{3} + \frac{1}{3}(x_2^3 - x_1^3) + g_c^4 \left( \frac{1}{x_1} - \frac{1}{x_2} \right) \right] - \frac{\omega_0}{2} \left( \frac{g_c}{\sqrt{3}\sigma} \right), & x_1 < -g_c \text{ and } x_2 > g_c, \\ -\frac{\omega_0}{2}, & |x_1| < g_c \text{ and } 0 < x_2 \leq g_c, \\ D_1 \left[ \frac{x_2^3}{3} - \frac{g_c^4}{x_2} + \frac{2g_c}{3} \right] - \frac{\omega_0}{2} \left( \frac{g_c - x_1}{2\sqrt{3}\sigma} \right), & |x_1| < g_c \text{ and } x_2 > g_c, \\ D_1 \left[ \frac{1}{3}(x_2^3 - x_1^3) + g_c^4 \left( \frac{1}{x_1} - \frac{1}{x_2} \right) \right], & x_1, x_2 > g_c, \text{ and } x_1 < x_2, \end{cases} \quad (\text{A1})$$

where  $D_1 = -\frac{1}{2\sqrt{3}\sigma\omega}$ . For the average boson number the disorder-averaged expression is

$$\frac{\overline{\langle a^\dagger a \rangle}}{N} = \begin{cases} D_2 \left[ -\frac{4g_c^2}{3} - \frac{x_1^3}{3g_c} - \frac{g_c^4}{x_1} \right], & x_1 < -g_c \text{ and } 0 < x_2 \leq g_c, \\ D_2 \left[ -\frac{8g_c^3}{3} + \frac{1}{3}(x_2^3 - x_1^3) + g_c^4 \left( \frac{1}{x_2} - \frac{1}{x_1} \right) \right], & x_1 < -g_c \text{ and } x_2 > g_c, \\ 0, & |x_1| < g_c \text{ and } 0 < x_2 \leq g_c, \\ D_2 \left[ \frac{x_2^3}{3} + \frac{g_c^4}{x_2} - \frac{4g_c^2}{3} \right], & |x_1| < g_c \text{ and } x_2 > g_c, \\ D_2 \left[ \frac{1}{3}(x_2^3 - x_1^3) + g_c^4 \left( \frac{1}{x_2} - \frac{1}{x_1} \right) \right], & x_1, x_2 > g_c, \text{ and } x_1 < x_2, \end{cases} \quad (\text{A2})$$

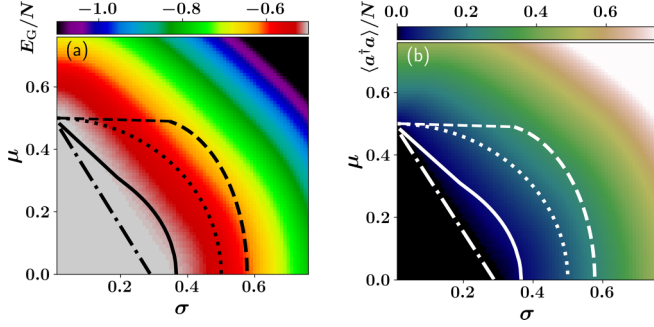


FIG. 6. Phase diagram which we calculate theoretically using Eq. (A1) and Eq. (A2) of the disordered Dicke model with uniform coupling distribution [Eq. (8)] considering the thermodynamic limit. To map it out, we show (a) the ground-state energy per atom  $E_G/N$  and (b) the average boson number per atom,  $\langle a^\dagger a \rangle/N$  wrt. the ground state, as a function of the standard deviation  $\sigma$  and the mean  $\mu$  of the coupling parameters  $g_i$ . We consider the resonant case  $\omega = \omega_0 = 1$ . The dot dashed line is given by Eq. (A9), the dashed line by Eq. (A11), the solid line by Eq. (A12), and the dotted line by Eq. (7). Here, Eq. (A9) is based on a solution of the Taylor series expansion of the disordered averaged observables, while we obtain Eqs. (A11) to (A12) using heuristics exploiting a symmetry of the Hamiltonian.

where  $D_2 = \frac{1}{2\sqrt{3}\sigma\omega^2}$ . In Fig. 6 we plot the disordered-averaged values of the ground-state energy [Fig. 6(a)] per atom and the average boson number in the ground state per atom [Fig. 6(b)] as a function of  $\mu$  and  $\sigma$  of the coupling parameter. Similar to the numerical data in Fig. 2 in the main text, in this figure also the white or pink color indicates the normal phase where the ground-state energy is large and constant  $\frac{E_G}{N} = -\frac{\omega_0}{2}$  and the other colors represent the superradiant phase where  $\frac{E_G}{N}$  is decreasing. Again in Fig. 6(b) the normal phase with  $\frac{\langle a^\dagger a \rangle}{N} \approx 0$  (black color) and the superradiant phase where  $\frac{\langle a^\dagger a \rangle}{N}$  is finite (other colors) are highlighted. Since intensive quantities are being shown, the dependence on  $N$  is explicitly absent, and therefore, we would expect this picture to hold in the thermodynamic limit. Comparing Figs. 2 and 6, we see that, in Fig. 6, the entire normal phase seems to become more homogeneous. Also the boundary separating the SP and NP is no longer so well captured by Eq. (7). We now attempt to obtain the phase boundary heuristically.

For the NP ( $|g| \leq g_c$ ) the third case is applicable and thus

$$\frac{\overline{E_G}}{N} = -\frac{\omega_0}{2}, \quad (\text{A3})$$

$$\frac{\langle a^\dagger a \rangle}{N} = 0. \quad (\text{A4})$$

However, for the SP ( $|g| > g_c$ ), we consider only the fourth case:  $|x_1| < g_c$  and  $x_2 > g_c$  for the QPT around  $g_c$ . Thus

$$\frac{\overline{E_G}}{N} = -\frac{1}{2\sqrt{3}\sigma\omega} \left[ \frac{x_2^3}{3} - \frac{g_c^4}{x_2} + \frac{2g_c}{3} \right] - \frac{\omega_0}{2} \left( \frac{g_c - x_1}{2\sqrt{3}\sigma} \right), \quad (\text{A5})$$

$$\frac{\langle a^\dagger a \rangle}{N} = \frac{1}{2\sqrt{3}\sigma\omega^2} \left[ \frac{x_2^3}{3} + \frac{g_c^4}{x_2} - \frac{4g_c^3}{3} \right]. \quad (\text{A6})$$

Taylor expanding around the critical point  $g_c$  and considering only the dominant terms, we have

$$\frac{\overline{E_G}}{N} \approx -\frac{\omega_0}{2} \left( \frac{g_c - x_1}{2\sqrt{3}\sigma} \right) - \frac{A\omega_0}{2} (x_2 - g_c) - 1.33A\omega_0 (x_2 - g_c)^3, \quad (\text{A7})$$

$$\frac{\langle a^\dagger a \rangle}{N} \approx \frac{A}{\omega^2} (x_2 - g_c)^2 - \frac{0.667A}{\omega^2} (x_2 - g_c)^3, \quad (\text{A8})$$

where  $A = \frac{1}{2\sqrt{3}\sigma}$  and  $x_2$  is the upper limit of the integration  $\mu + \sqrt{3}\sigma$ . At the critical point the scaled ground-state energy is  $-\frac{\omega_0}{2}$  and the scaled average boson number is zero, hence we have a relation for the critical line as a function of  $\mu$  and  $\sigma$ :

$$\mu + \sqrt{3}\sigma = g_c. \quad (\text{A9})$$

The dash-dotted line in Fig. 6 represents the quantum critical line which is given in Eq. (A9) and our analytical data already roughly agrees with this linear relation. It is remarkable that the formula describes the numerical data this well, despite the coarse approximation of just disorder-averaging the clean Dicke model results. Around the critical line the expectation value (with respect to the uniform disorder) of the ground-state energy and the average boson number can be represented by the simpler Taylor series in Eqs. (A7) and (A8), respectively.

The line that separates the NP and the SP in Fig. 6 can also be obtained approximately with the aid of a heuristic argument that exploits a symmetry of the Hamiltonian, which we described in the main text [see Eq. (6)]. Since it is the magnitude of the couplings that matters, we have already seen that working with the rms value of  $g$  yields a good estimate for the line separating the SP and the NP. An alternate way to proceed is to work with an effective distribution where the weight corresponding to a negative value of the coupling is shifted to its positive value. Hence when the lower limit of the uniform distribution  $\mu - \sqrt{3}\sigma < 0$  the effective distribution is

$$P_{\text{eff}}(g) = \begin{cases} \frac{1}{\sqrt{3}\sigma} & \text{if } 0 < g < -(\mu - \sqrt{3}\sigma), \\ \frac{1}{2\sqrt{3}\sigma} & \text{if } -(\mu - \sqrt{3}\sigma) < g < (\mu + \sqrt{3}\sigma), \end{cases} \quad (\text{A10})$$

as shown in Fig. 7(a). The effective distribution in this case yields a mean value of  $\langle g \rangle = \frac{\mu^2 + 3\sigma^2}{2\sqrt{3}\sigma}$  and a variance of  $\langle g^2 \rangle = \mu^2 + \sigma^2$ , which, in turn, corresponds to a standard deviation of:  $\sqrt{\mu^2 + \sigma^2 - \frac{(\mu^2 + 3\sigma^2)^2}{12\sigma^2}}$ . If the lower limit of the distribution  $\mu - \sqrt{3}\sigma \geq 0$ , the effective distribution remains identical to the original one and its mean and standard deviation remain unchanged as  $\mu$  and  $\sigma$  [Fig. 7(b)].

To identify the phase transition line heuristically, we argue as follows. We would expect that as more and more of the couplings  $g_i$  are drawn above  $g_c$ , we would see increasingly dominant effects characteristic of the SP. A coarse way to identify this would be to simply demand that the rightmost edge of the effective distribution [Eq. (A10)] must be above the critical coupling  $g_c = \frac{1}{2}$ , i.e.,  $\mu + \sqrt{3}\sigma = g_c$ , which is nothing but the crude approximation Eq. (A9) and dot-dashed line in Fig. 6. For a refined result, we demand that the mean

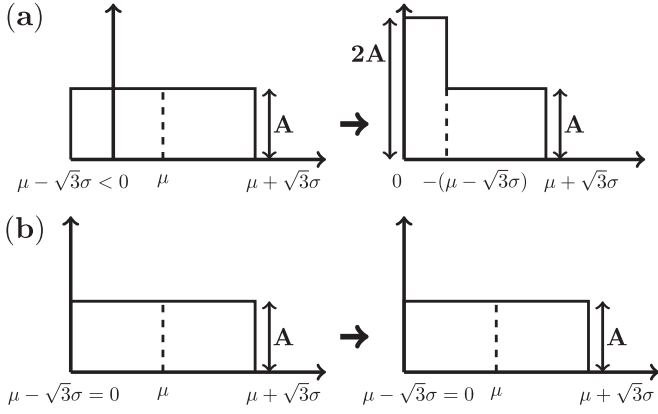


FIG. 7. Effective distribution containing only positive coupling strengths. The left panel denotes the original distribution, whereas the right panel shows the effective distribution where only the absolute values of the coupling strengths are considered. (a) For  $\mu - \sqrt{3}\sigma < 0$ , the effective mean of the coupling strength is  $\langle g \rangle = \frac{\mu^2 + 3\sigma^2}{2\sqrt{3}\sigma}$  and the effective variance  $\langle g^2 \rangle = \mu^2 + \sigma^2$  hence the effective standard deviation is  $\sqrt{\mu^2 + \sigma^2 - \frac{(\mu^2 + 3\sigma^2)^2}{12\sigma^2}}$ . (b) For  $\mu - \sqrt{3}\sigma \geq 0$  the distribution remains unchanged: the mean and the standard deviation of  $g$  are  $\mu$  and  $\sigma$ . For both cases  $A = \frac{1}{2\sqrt{3}\sigma}$ .

of the effective distribution [Eq. (A10)] must reach above  $g_c$

$$\frac{\mu^2 + 3\sigma^2}{2\sqrt{3}\sigma} = g_c, \quad \mu < \sqrt{3}\sigma, \quad (A11)$$

$$\mu = g_c, \quad \mu \geq \sqrt{3}\sigma.$$

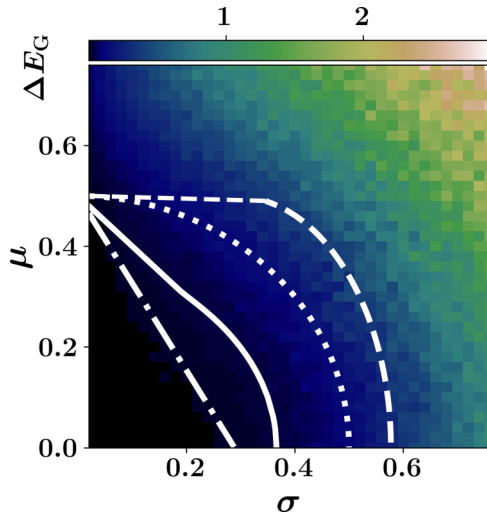


FIG. 8. Phase diagram of the disordered Dicke model with uniform coupling distribution [Eq. (8)]. To map it out, we show the ground-state energy fluctuations  $\Delta E_G = \sqrt{\langle E_G^2 \rangle - \langle E_G \rangle^2}$ , as a function of the standard deviation  $\sigma$  and the mean  $\mu$  of the coupling parameters  $g_i$ . We consider the resonant case  $\omega = \omega_0 = 1$ , take the average over 120 realizations, fix the atom number to be  $N = 8$ , and the bosonic cutoff to be  $n_{\max} = 40$ . The dot dashed line is given by Eq. (A9), the dashed line by Eq. (A11), the solid line by Eq. (A12), and the dotted line by Eq. (7). Here, Eq. (A9) is based on a solution of the Taylor series expansion of the disordered averaged observables, while we obtain Eqs. (A11) and (A12) using heuristics exploiting a symmetry of the Hamiltonian.

This is shown by the dashed line in Fig. 6. A less stringent condition is to demand that the mean plus one standard deviation of the effective distribution [Eq. (A10)] must reach above  $g_c$ ,

$$\frac{\mu^2 + 3\sigma^2}{2\sqrt{3}\sigma} + \sqrt{\mu^2 + \sigma^2 - \frac{(\mu^2 + 3\sigma^2)^2}{12\sigma^2}} = g_c, \quad \mu < \sqrt{3}\sigma, \quad (A12)$$

$$\mu + \sigma = g_c, \quad \mu \geq \sqrt{3}\sigma.$$

This is shown by the solid white line in Fig. 6 and appears to be closest to the actual line of separation between the SP and NP.

While we studied the ground-state energy to characterize the phases in the main part of the paper, it is also interesting to look at the fluctuations in the ground-state energy  $\Delta E_G = \sqrt{\langle E_G^2 \rangle - \langle E_G \rangle^2}$ . Figure 8 shows the numerically computed values of the ground-state energy fluctuation of a small-sized system as a function of the standard deviation ( $\sigma$ ) and mean ( $\mu$ ) of the coupling parameter. In this figure, the black color indicates the normal phase where  $\Delta E_G$  is zero and the other colors represent the superradiant phase where  $\Delta E_G$  is increasing. We observe that the separation of the phases indicated by the energy fluctuations is in good agreement with the analytical results of Fig. 6.

## APPENDIX B: FINITE-SIZE ANALYSIS FOR THE UNIFORM DISTRIBUTION

Our numerical analysis is based on exact diagonalization as the total angular momentum is not conserved here. The

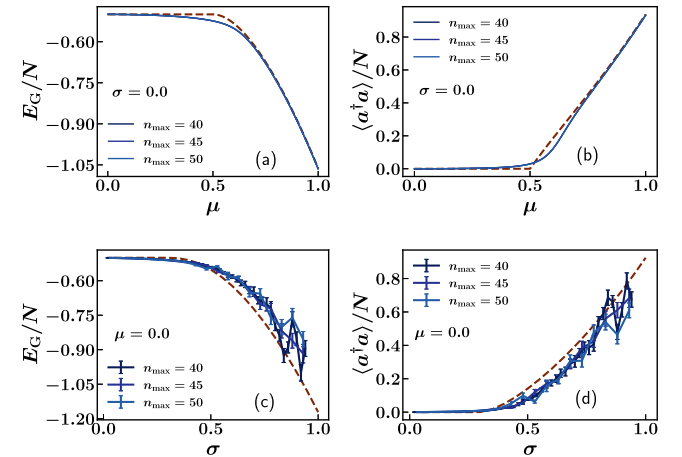


FIG. 9. [(a), (c)] The ground-state energy per atom  $E_G/N$  and [(b), (d)] the average boson number per atom,  $\langle a^\dagger a \rangle/N$  wrt. the ground state, as a function of [(a), (b)] the mean  $\mu$  and [(c), (d)] the standard deviation  $\sigma$  of the coupling parameters  $g_i$ . We consider the resonant case  $\omega = \omega_0 = 1$ , take the average over 60 realizations, fix the atom number  $N = 8$ , and vary the bosonic cutoff  $n_{\max} = 40, 45, 50$ . Here we consider the disordered Dicke model with uniform coupling distribution. The solid lines denote the numerical disordered average value whereas the dashed lines correspond to the analytical value in the thermodynamic limit.

total Hilbert space dimension is  $N_D = 2^N(n_{\max} + 1)$ , where the bosonic cutoff  $n_{\max}$  has to be introduced. Due to computational constraints, we cannot consider very large values for the bosonic cutoff. However, it is useful to make a systematic study of our various results as a function of  $n_{\max}$ . In Fig. 9 we compare the numerical disordered-averaged data for a small system with  $N = 8$  atoms (solid lines in Fig. 9) with the corresponding theoretical value (dashed lines in Fig. 9) obtained from Eqs. (A1) and (A2). In Fig. 9 we keep the atom number fixed at  $N = 8$  and gradually increase the bosonic cutoff  $n_{\max}$ . Figures 9(a) and 9(c) show the ground-state energy of the system per atom and Figs. 9(b) and 9(d) show the average boson number per atom. For the top panel [Figs. 9(a) and 9(b)] we fix the standard deviation of the coupling strength ( $g$ ) and plot the disorder-averaged observables as a function of the mean of  $g$ ,

corresponding to a vertical cut through Fig. 2. For the bottom panel, we instead consider horizontal cuts. For both cases, we see a clear quantum phase transition at some critical point in the analytical calculations, with the numerical data strongly supportive of the theoretical values. The top row is equivalent to the usual QPT in the clean isotropic Dicke model. However, from the bottom row of panels we conclude that coupling strength disorder with a sufficiently broad distribution causes a QPT even for vanishing mean coupling  $\mu = \langle g \rangle = 0$ . We see that the ground-state energy and average boson number at  $N = 8$  retain clear evidence of the QPT found from analytical calculations in the large system limit, even though the bosonic cutoff is limited to  $n_{\max} = 40$ . In Fig. 9, we show the data for a uniform distribution but we find similar behavior for other distributions.

- 
- [1] R. H. Dicke, Coherence in spontaneous radiation processes, *Phys. Rev.* **93**, 99 (1954).
- [2] C. Emary and T. Brandes, Quantum chaos triggered by precursors of a quantum phase transition: The Dicke model, *Phys. Rev. Lett.* **90**, 044101 (2003).
- [3] C. Emary and T. Brandes, Chaos and the quantum phase transition in the Dicke model, *Phys. Rev. E* **67**, 066203 (2003).
- [4] N. Lambert, C. Emary, and T. Brandes, Entanglement and the phase transition in single-mode superradiance, *Phys. Rev. Lett.* **92**, 073602 (2004).
- [5] K. Baumann, C. Guerlin, F. Brennecke, and T. Esslinger, Dicke quantum phase transition with a superfluid gas in an optical cavity, *Nature (London)* **464**, 1301 (2010).
- [6] P. Kirton, M. M. Roses, J. Keeling, and E. G. Dalla Torre, Introduction to the Dicke model: from equilibrium to nonequilibrium, and vice versa, *Adv. Quantum Technol.* **2**, 1800043 (2019).
- [7] P. Pérez-Fernández and A. Relaño, From thermal to excited-state quantum phase transition: The Dicke model, *Phys. Rev. E* **96**, 012121 (2017).
- [8] P. Das and A. Sharma, Revisiting the phase transitions of the Dicke model, *Phys. Rev. A* **105**, 033716 (2022).
- [9] Y. K. Wang and F. T. Hioe, Phase transition in the Dicke model of superradiance, *Phys. Rev. A* **7**, 831 (1973).
- [10] G.-L. Zhu, X.-Y. Lü, S.-W. Bin, C. You, and Y. Wu, Entanglement and excited-state quantum phase transition in an extended Dicke model, *Front. Phys.* **14**, 52602 (2019).
- [11] P. Cejnar, P. Stránský, M. Macek, and M. Kloc, Excited-state quantum phase transitions, *J. Phys. A: Math. Theor.* **54**, 133001 (2021).
- [12] M. Gross and S. Haroche, Superradiance: An essay on the theory of collective spontaneous emission, *Phys. Rep.* **93**, 301 (1982).
- [13] H. Carmichael, C. Gardiner, and D. Walls, Higher order corrections to the Dicke superradiant phase transition, *Phys. Lett. A* **46**, 47 (1973).
- [14] G. C. Duncan, Effect of antiresonant atom-field interactions on phase transitions in the Dicke model, *Phys. Rev. A* **9**, 418 (1974).
- [15] H. T. Quan and F. M. Cucchietti, Quantum fidelity and thermal phase transitions, *Phys. Rev. E* **79**, 031101 (2009).
- [16] M. A. Bastarrachea-Magnani, A. Relaño, S. Lerma-Hernández, B. L. del Carpio, J. Chávez-Carlos, and J. G. Hirsch, Adiabatic invariants for the regular region of the Dicke model, *J. Phys. A: Math. Theor.* **50**, 144002 (2017).
- [17] V. V. Temnov and U. Woggon, Superradiance and subradiance in an inhomogeneously broadened ensemble of two-level systems coupled to a low- $q$  cavity, *Phys. Rev. Lett.* **95**, 243602 (2005).
- [18] F. M. Marchetti, J. Keeling, M. H. Szymańska, and P. B. Littlewood, Thermodynamics and excitations of condensed polaritons in disordered microcavities, *Phys. Rev. Lett.* **96**, 066405 (2006).
- [19] F. M. Marchetti, J. Keeling, M. H. Szymańska, and P. B. Littlewood, Absorption, photoluminescence, and resonant rayleigh scattering probes of condensed microcavity polaritons, *Phys. Rev. B* **76**, 115326 (2007).
- [20] I. Diniz, S. Portolan, R. Ferreira, J. M. Gérard, P. Bertet, and A. Auffèves, Strongly coupling a cavity to inhomogeneous ensembles of emitters: Potential for long-lived solid-state quantum memories, *Phys. Rev. A* **84**, 063810 (2011).
- [21] O. Tsyplatyev and D. Loss, Dynamics of the inhomogeneous Dicke model for a single-boson mode coupled to a bath of nonidentical spin-1/2 systems, *Phys. Rev. A* **80**, 023803 (2009).
- [22] E. Cortese, P. G. Lagoudakis, and S. De Liberato, Collective optomechanical effects in cavity quantum electrodynamics, *Phys. Rev. Lett.* **119**, 043604 (2017).
- [23] J. Keeling and P. G. Kirton, Orientational alignment in cavity quantum electrodynamics, *Phys. Rev. A* **97**, 053836 (2018).
- [24] H. S. Dhar, M. Zens, D. O. Krimer, and S. Rotter, Variational renormalization group for dissipative spin-cavity systems: Periodic pulses of nonclassical photons from mesoscopic spin ensembles, *Phys. Rev. Lett.* **121**, 133601 (2018).
- [25] D. O. Krimer, S. Putz, J. Majer, and S. Rotter, Non-markovian dynamics of a single-mode cavity strongly coupled to an inhomogeneously broadened spin ensemble, *Phys. Rev. A* **90**, 043852 (2014).
- [26] D. O. Krimer, M. Zens, S. Putz, and S. Rotter, Sustained photon pulse revivals from inhomogeneously broadened spin ensembles, *Laser Photonics Rev.* **10**, 1023 (2016).
- [27] Z. Zhang, C. H. Lee, R. Kumar, K. J. Arnold, S. J. Masson, A. L. Grimsmo, A. S. Parkins, and M. D. Barrett, Dicke-model

- simulation via cavity-assisted Raman transitions, *Phys. Rev. A* **97**, 043858 (2018).
- [28] V. Vedral, Classical correlations and entanglement in quantum measurements, *Phys. Rev. Lett.* **90**, 050401 (2003).
- [29] D. P. DiVincenzo, M. Horodecki, D. W. Leung, J. A. Smolin, and B. M. Terhal, Locking classical correlations in quantum states, *Phys. Rev. Lett.* **92**, 067902 (2004).
- [30] G. Adesso and A. Datta, Quantum versus classical correlations in gaussian states, *Phys. Rev. Lett.* **105**, 030501 (2010).
- [31] P. Das, D. S. Bhakuni, and A. Sharma, Phase transitions of the anisotropic Dicke model, *Phys. Rev. A* **107**, 043706 (2023).
- [32] F. T. Hioe, Phase transitions in some generalized Dicke models of superradiance, *Phys. Rev. A* **8**, 1440 (1973).
- [33] P. Rotondo, M. Cosentino Lagomarsino, and G. Viola, Dicke simulators with emergent collective quantum computational abilities, *Phys. Rev. Lett.* **114**, 143601 (2015).
- [34] G. Rainò, M. A. Becker, M. I. Bodnarchuk, R. F. Mahrt, M. V. Kovalenko, and T. Stöferle, Superfluorescence from lead halide perovskite quantum dot superlattices, *Nature (London)* **563**, 671 (2018).
- [35] F. Dimer, B. Estienne, A. S. Parkins, and H. J. Carmichael, Proposed realization of the Dicke-model quantum phase transition in an optical cavity QED system, *Phys. Rev. A* **75**, 013804 (2007).
- [36] J. Maziero, H. C. Guzman, L. C. Céleri, M. S. Sarandy, and R. M. Serra, Quantum and classical thermal correlations in the XY spin- $\frac{1}{2}$  chain, *Phys. Rev. A* **82**, 012106 (2010).
- [37] J. P. Dowling and G. J. Milburn, Quantum technology: the second quantum revolution, *Philos. Trans. R. Soc. London A* **361**, 1655 (2003).
- [38] A. Neuzner, M. Körber, O. Morin, S. Ritter, and G. Rempe, Interference and dynamics of light from a distance-controlled atom pair in an optical cavity, *Nat. Photonics* **10**, 303 (2016).
- [39] T. Puppe, I. Schuster, A. Grothe, A. Kubanek, K. Murr, P. W. H. Pinkse, and G. Rempe, Trapping and observing single atoms in a blue-detuned intracavity dipole trap, *Phys. Rev. Lett.* **99**, 013002 (2007).
- [40] R. V. Krems, Molecules near absolute zero and external field control of atomic and molecular dynamics, *Int. Rev. Phys. Chem.* **24**, 99 (2005).
- [41] L. D. Carr, D. DeMille, R. V. Krems, and J. Ye, Cold and ultracold molecules: science, technology and applications, *New J. Phys.* **11**, 055049 (2009).
- [42] F. Herrera and F. C. Spano, Cavity-controlled chemistry in molecular ensembles, *Phys. Rev. Lett.* **116**, 238301 (2016).
- [43] P. Badankó, G. J. Halász, L. S. Cederbaum, Á. Vibók, and A. Csehi, Communication: Substantial impact of the orientation of transition dipole moments on the dynamics of diatomics in laser fields, *J. Chem. Phys.* **149**, 181101 (2018).
- [44] Y. Hao, L. F. Pašteka, L. Visscher, P. Aggarwal, H. L. Bethlem, A. Boeschoten, A. Borschevsky, M. Denis, K. Esajas, S. Hoekstra *et al.*, High accuracy theoretical investigations of CaF, SrF, and BaF and implications for laser-cooling, *J. Chem. Phys.* **151**, 034302 (2019).
- [45] B. K. Stuhl, B. C. Sawyer, D. Wang, and J. Ye, Magneto-optical trap for polar molecules, *Phys. Rev. Lett.* **101**, 243002 (2008).
- [46] E. S. Shuman, J. F. Barry, and D. DeMille, Laser cooling of a diatomic molecule, *Nature (London)* **467**, 820 (2010).